This article has been accepted for inclusion in a future issue of this journal. Content is final as presented, with the exception of pagination.

Backstepping Control of Smart Grid-Connected Distributed Photovoltaic Power Supplies for Telecom Equipment

Aranzazu D. Martin, *Student Member, IEEE*, J. M. Cano, J. Fernando A. Silva, *Senior Member, IEEE*, and Jesús R. Vázquez, *Member, IEEE*

***Abstract*—Backstepping controllers are obtained for distributed hybrid photovoltaic (PV) power supplies of telecommunication equipment. Grid-connected PV-based power supply units may contain dc–dc buck–boost converters linked to single-phase inverters. This distributed energy resource operated within the self-consumption concept can aid in the peak-shaving strategy of ac smart grids. New backstepping control laws are obtained for the single-phase inverter and for the buck–boost converter feeding a telecom equipment/battery while sourcing the PV excess power to the smart grid or to grid supply the telecom system. The backstepping approach is robust and able to cope with the grid nonlinearity and uncertainties providing dc input current and voltage controllers for the buck–boost converter to track the PV panel maximum power point, regulating the PV output dc voltage to extract maximum power; unity power factor sinusoidal ac smart grid inverter currents and constant dc-link voltages suited for telecom equipment; and inverter bidirectional power transfer. Experimental results are obtained from a lab setup controlled by one inexpensive dsPIC running the sampling, the backstepping and modulator algorithms. Results show the controllers guarantee maximum power transfer to the telecom equipment/ac grid, ensuring steady dc-link voltage while absorbing/injecting low harmonic distortion current into the smart grid.**

***Index Terms*—Backstepping, buck–boost converter, dc/ac converter, MPPT, self-consumption, smart grids.**

I. Introduction

PHOTOVOLTAIC (PV) energy is now widely used to supply electricity to isolated houses and autonomous devices and to generate electrical energy to inject into power grids. The solar cells are connected in series strings and then paralleled to obtain a solar array or module. The common grid-connected PV system consists of solar modules, a step-up dc–dc converter and a dc–ac converter. The dc power generated by the solar cells arrays is temperature and irradiance dependent, the dc–dc converter being mandatory to regulate the PV panel output voltage in order to stay in its maximum power point (MPP) [1]. The PV system is connected to a load or can be interfaced to the electrical grid using a dc–ac converter to inject a sinusoidal current in phase with the voltage of the electrical network. Combining solar modules in series and in parallel creates PV panels able to supply power to help shave midday peaks of grid power consumption of centralized energy as renewable distributed energy resources (DER).

When the number of needed panels is large, shadowing in some panels strongly reduces the overall power output. Given that individual PV panels usually output a few hundred watts, for most applications it is desirable to seek for a distributed PV architecture in which each PV panel has its own dc–dc converter to locally optimize the MPP even considering partial shadowing, ageing, or different operating conditions [1], [2]. The distributed dc–dc converters outputs are then connected in parallel to feed a load or the grid through one or several distributed inverters (dc microgrid connected to an ac grid). The distributed option ensures higher reliability concerning converter failures or ageing in the converter modules or solar panels, and their smaller individual dc capacitors can be chosen to ensure extended lifetimes.

Under the concept of self-consumption of electrical power, each electricity consumer should be given the possibility to connect a PV system able to produce the energy corresponding to the consumer average consumption. This energy could be used in the producer–consumer (*prosumer*) site and the short-term available surplus injected in the electrical grid. In this case, the *prosumer* receives a payment for the excess electricity generated regarding the amount consumed within a billing period [3], [4].

Inserting energy storage systems in the low voltage (LV) grid, close to the *prosumers* site, [community energy storage—(CES)], increases the global value of the storage solution [5].

PV systems are advantageous for the smart grid concept as they can supply or store the extra power during the midday peak power consumption hours, while the *prosumer* can rely on CES or grid electricity during sunless hours, leveling the centralized injected grid power. This concept, together with the mitigation of voltage rise caused by DER is central toward a LV ac smart grid [6], with power converters buffering and smoothing DER intermittency, avoiding reverse power flow to the medium-voltage network, providing voltage support, spinning reserve, power factor correction, harmonic filtering, uninterruptible power supply, peak shaving, load leveling to defer capacity upgrade.

Manuscript received December 14, 2014; revised April 8, 2015; accepted May 5, 2015. This work was supported in part by the Ministerio de Educación, Cultura y Deporte of Spain, under the Formación del Profesorado Universitario (FPU) grant, and in part by Portugal funds through Fundação para a Ciência e a Tecnologia (FCT) with reference UID/CEC/50021/2013. Paper no. TEC-00841-2014.

A. D. Martin, J. M. Cano, and J. R. Vazquez are with the Electrical Engineering Department, University of Huelva, 21710 Huelva, Spain (e-mail: aranzazu.delgado@die.uhu.es; juadiacan@alum.us.es; vazquez@uhu.es).

J. F. A. Silva is with Instituto de Engenharia de Sistemas e Computadores - Investigação e Desenvolvimento (INESC-ID), Instituto Superior Técnico, Universidade de Lisboa, 1649-004 Lisboa, Portugal (e-mail: fernandos@alfa.ist.utl.pt).

Color versions of one or more of the figures in this paper are available online at http://ieeexplore.ieee.org.

Digital Object Identifier 10.1109/TEC.2015.2431613

0885-8969 © 2015 IEEE. Personal use is permitted, but republication/redistribution requires IEEE permission.
See http://www.ieee.org/publications_standards/publications/rights/index.html for more information.

This article has been accepted for inclusion in a future issue of this journal. Content is final as presented, with the exception of pagination.

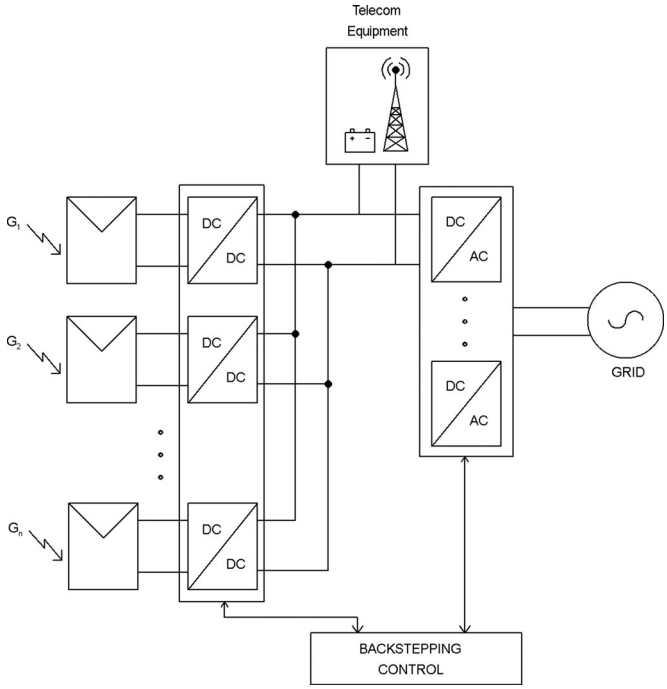

Fig. 1. PV distributed hybrid self-consumption system and telecom load.

The self-consumption concept is well suited for telecommunications applications, since telecom apparatus power consumption is roughly constant. Excess PV energy during sun hours can also be used to shave the smart grid consumption peaks in the evening if back-up storage batteries or CES are used.

In this paper, a telecom load is connected between the distributed PV panel dc–dc converter and the dc–ac converter (see Fig. 1). This PV system is suitable for LV telecommunication apparatus, where the nominal voltage is usually 48 V, but can vary in the range from 36 to 75 V [7]. Since most PV panels present output voltages nearly in the same range, from the available dc–dc converter topologies [8], a buck–boost (step-up/down) dc–dc converter [8] is selected, as it can supply voltages in the above range, having input voltages inside the same range or even lower or higher than the range limits.

Smart grid-connected PV systems require dc–ac converters to connect the system to the power grid [6], [9], [10]. Hybrid ac–dc microgrids can integrate CES and DER based on renewable energy sources, where the power electronics interfaces between ac bus and dc bus should be controlled so that the microgrid works under different operation modes (isolated or controlling the generation and consumption) [11].

In this paper, a single-phase dc–ac converter [8] has been used and controlled to inject nearly sinusoidal currents (to reduce harmonic distortion) in phase with the LV–ac grid. Within the self-consumption concept, this converter must work as an inverter or as a unity power factor rectifier (reversible operation) depending on the telecom load power requirement, on the PV panel power generated and on the telecom/battery load needs. During the hours where the telecom application requires more power than the PV system can generate the dc–ac converter works as a rectifier to complement the PV panel that cannot produce the needed power due to low irradiance levels. At midday hours, the excess power produced by the PV panels can be used to recharge the back-up battery or be injected in the grid after battery recharge, the dc–ac converter working as an inverter. Additionally, if there is a fault in the grid, leading to voltage sag, the PV panel and battery of this hybrid power system will continue to power the load that will not be affected by the sag.

The control strategy must be designed to operate the PV panel in the MPP to obtain maximum power transfer. There are different MPP tracking (MPPT) algorithms [12] to reach the MPP [1]. The most used algorithm is the Perturb and Observe (P&O) method [1]. Several other algorithms, such as the incremental conductance [13], the ripple correlation control [14], the sliding mode control [1], or MPP trackers based on artificial neuronal networks, or fuzzy logic [15], [16], have been introduced amongst others [17].

Due to the oscillatory behavior of the P&O method and the required processing time of advanced MPPT algorithms, a nonlinear control method is proposed to achieve the MPP, the backstepping control [18], [19]. Besides, instead of linear proportional–integral (PI) compensators to regulate the dc microgrid voltage at the input of the inverter in order to inject sinusoidal currents to the LV grid [20]–[22], the backstepping method is shown to generate original and new controllers for the dc–ac converter considering the single-phase converter slow and fast dynamics. Dynamics separation is needed as the grid power injected/retrieved by a single-phase inverter is not constant during a grid period. The backstepping method guarantees stable and robust operation as an inverter (minimum phase system) or as a rectifier (nonminimum phase system), being also able to cope with the ac grid voltage variations and microgrid operating modes [11].

Previous works [22], [23] have derived the backstepping and the adaptive backstepping MPPT algorithm for the buck–boost, without considering the single-phase inverter dynamics, as the dynamic separation, which is a crucial contribution of this paper, was not used. Therefore, in the simulation results published, a hysteresis current controlled three-phase inverter (constant power) with a PI voltage controller had to be used in [22] and [23] to inject all the PV array power into the grid. Powering loads in the dc grid was not considered in [22] and [23].

The advantages of backstepping controllers are related to the use of the converters model direct dynamics, and Lyapunov functions to guarantee the stability and robustness of the system, therefore enhancing the system performance.

After modeling the converter association (see Section II), this paper presents the backstepping control (see Section III) of the buck–boost converter and dc–ac converter, solves the problem of applying backstepping to dc–ac reversible converters with both fast and slow dynamics. Instead of using known platforms using acquisition and control expensive commercial boards [24], a lab setup has been built to check the performance of the proposed backstepping controllers, including a PV panel simulator, a buck–boost converter, 48-V load, and a grid-connected single-

This article has been accepted for inclusion in a future issue of this journal. Content is final as presented, with the exception of pagination.

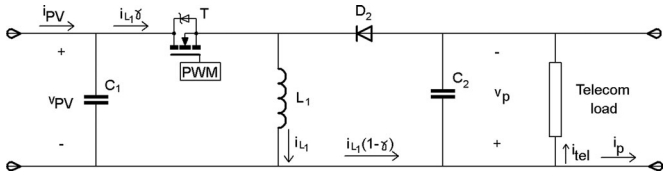

Fig. 2. Buck–boost converter with input filtering capacitor and load.

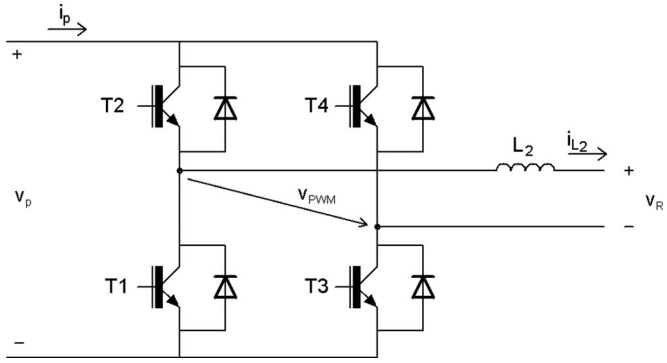

Fig. 3. Single-phase dc–ac inverter.

phase full-bridge inverter, all the converters and MPP being implemented in a low-cost dsPIC microcontroller. Section IV shows this experimental setup and discusses experimental results, while Section V summarizes the main results.

II. Self-Consumption PV System Modeling

A self-consumption smart grid-connected PV system may contain several PV panels able to convert power in excess of the needed by the telecom load during midday hours. Distributed hybrid architectures [25]–[27] can use one dc–dc power converter per PV panel, and one or several single-phase dc–ac power inverters/rectifiers, smart grid connected, that are controlled to power up the telecom loads when there is not enough sun available.

A. DC–DC Buck–Boost Modeling

The dc–dc buck–boost power converter (see Fig. 2) has a filtering capacitor connected to the output voltage $v_{\rm PV}$ of the PV panel and is controlled to ensure the voltage $v_{\rm PV}$ across this capacitor equals the maximum power voltage ($V_{\rm MPP}$), therefore transferring the maximum power from the solar array. The buck–boost converter is driven by a fixed frequency pulse width modulation (PWM) duty-cycle generator with duty cycle γ, $\gamma \in]\,0,\,1[$. In addition to the input capacitor, the converter has an inductor and output capacitor as well as a low-ON-state voltage drop MOSFET and Schottky diode for loss minimization.

v_p is the buck–boost converter output voltage in V, $i_{\rm PV}$ is the PV panel output current in A, $i_{L_1}\,(1-\gamma)$ is the output current in A, i_{L1} is the inductor current in A, assuming ideal semiconductors and continuous-conduction mode (CCM) operation. The telecom load current $i_{\rm tel}$ is considered to be a disturbance.

Using state-switching period averaged values, the buck–boost converter dynamics are as follows:

$$\frac{dv_{\rm PV}}{dt} = i_{\rm PV}/C_1 - \gamma i_{L_1}/C_1 \tag{1}$$

$$\frac{di_{L_1}}{dt} = \gamma\, v_{\rm PV}/L_1 - (1-\gamma)v_p/L_1 \tag{2}$$

$$\frac{dv_p}{dt} = \left(i_{L_1}(1-\gamma) - i_p - i_{\rm tel}\right)/C_2 \tag{3}$$

where i_p in (3) is the inverter dc current.

B. DC–AC Power Converter Modeling

Consider also that the single-phase dc–ac converter input voltage (see Fig. 3) is the buck–boost converter output voltage v_p to be controlled by the dc–ac converter to be almost constant voltage of the supplied telecom load. The dc–ac converter is driven using a three level PWM sinusoidal modulator in order to control the dc voltage v_p by changing the alternating current i_{L2} to be injected in the network at voltage v_R.

The dc–ac converter dynamics (4) (5) can be written in a strict-feedback form as

$$C_2\frac{dv_p^2}{2dt} = i_p v_p - i_{L_2} v_R \tag{4}$$

$$L_2\frac{di_{L_2}}{dt} = \beta\, v_p - v_R. \tag{5}$$

Equation (4) represents the energy transfer through the dc–ac converter, considering it is conservative and operates at unity power factor. In (5), the function that converts the dc–ac converter switched voltage $v_{\rm PWM}$ to the fundamental sinusoidal voltage is the sinusoidal modulation waveform β. Equations (4) and (5) will be used to define the dc–ac converter slow and fast dynamics, respectively.

If the PV array supplies excess power, that excess will tend to increase the v_p voltage. Then the dc–ac converter is operated as an inverter injecting the excess power in the electrical network to which it is connected using a step-down transformer. Oppositely, if the PV array delivers less power than the needed, then the dc–ac converter operates as a PWM rectifier sinking power from the electrical network.

In inverter mode, the dc–ac converter must inject a nearly sinusoidal current (to prevent harmonic distortion) in phase with the network voltage. In the rectifier mode, the ac current should have opposite phase relative to the network voltage.

III. Backstepping Control of the PV System

A nonlinear backstepping approach [18] is used to obtain the control laws for the dc–dc converter and the dc–ac converter. The backstepping method first calculates the fictitious or virtual control input i_{L1} to stabilize the lower order subsystem (1) at the origin, and then finds a way to calculate γ to enforce the dynamics in (2) necessary to track the i_{L1} value required to stabilize (1). The algorithm steps backward from (2) until the ultimate control γ is obtained. Compared to linear controllers, better results can be obtained since backstepping applies a recur-

This article has been accepted for inclusion in a future issue of this journal. Content is final as presented, with the exception of pagination.

sive methodology to the model direct dynamics and Lyapunov functions to guarantee the system stability and robustness.

A. Buck–Boost Converter Control

Usually, a buck–boost converter is controlled so that its output v_p voltage presents a constant reference value. However, in this self-consumption PV system, the purpose of the buck–boost backstepping controller is to define the converter duty cycle so that the converter regulates its input voltage to enforce the PV panel operation at the MPP. To accomplish this, the backstepping input $v_{\rm PV}$ voltage outer loop defines the inductor current reference value $i_{L_1\rm ref}$ to control the inductor i_{L1} current, and a recursively obtained inner current loop defines the needed duty cycle to track $i_{L_1\rm ref}$.

To apply the backstepping method [28] and stabilize the buck–boost to the origin (zero error), first the tracking error $e_{\rm PV}$ is defined to enforce the buck–boost input voltage $v_{\rm PV}$ to track the PV array MPP reference voltage $v_{\rm PVref}$ (zero tracking error)

$$e_{\rm PV} = v_{\rm PV} - v_{\rm PVref}. \tag{6}$$

Using the model (1) to calculate the time derivative of $e_{\rm pv}$ in (6), we obtain

$$\frac{de_{\rm PV}}{dt} = i_{\rm PV}/C_1 - (i_{L_1}\gamma)/C_1 - \frac{dv_{\rm PVref}}{dt}. \tag{7}$$

In this equation i_{L1} can be determined to be the stabilizing control input (or the virtual control law [18]) and the current reference for the inner loop. Now, a Lyapunov function globally positive definite and radially unbounded for all $e_{\rm PV}$ is selected

$$V_v = e_{\rm PV}^2/2. \tag{8}$$

To guarantee that the solution is globally asymptotically stable, the time derivative of the Lyapunov function $\frac{dV_v}{dt}$ must be globally negative definite for all $e_{\rm PV}$ [28]. Therefore, $e_{\rm PV}\frac{de_{\rm PV}}{dt} < 0$, a condition that can be enforced using

$$\begin{aligned}&\frac{de_{\rm PV}}{dt} = -k_{\rm PV}e_{\rm PV} \Rightarrow \\ &\Rightarrow i_{\rm PV}/C_1 - (i_{L_1}\gamma)/C_1 - \frac{dv_{\rm PVref}}{dt} = -k_{\rm PV}e_{\rm PV}.\end{aligned} \tag{9}$$

If $k_{\rm PV}$ in (9) is constant and positive, then $\frac{dV_v}{dt} < 0$ is verified. Supposing zero tracking error, the reference current $i_{L1\rm ref}$, for the virtual control law i_{L1} (stabilizing function), obeys $i_{L1\rm ref} = i_{L1}$, and can be obtained from (9), since $0 < \gamma < 1$

$$i_{L_1\rm ref} = \left(C_1 k_{\rm PV}e_{\rm PV} + i_{\rm PV} - C_1\frac{dv_{\rm PVref}}{dt}\right)/\gamma. \tag{10}$$

The reference current for the inner loop ($i_{L_1\rm ref} \neq 0$) is a function of the buck–boost modulator duty cycle γ. To define this duty cycle, a second feedback loop enforcing $i_{L_1} = i_{L_1\rm ref}$ is needed. The inductor current i_{L_1} should be equal to $i_{L_1\rm ref}$ to achieve a zero-tracking error defined as $e_{i_L 1} = i_{L_1} - i_{L_1\rm ref}$. Its time derivative is

$$\frac{de_{i_{L1}}}{dt} = \frac{di_{L_1}}{dt} - \frac{di_{L_1\rm ref}}{dt}. \tag{11}$$

The $i_{L1\rm ref}$ time derivative $\frac{di_{L_1\rm ref}}{dt}$ is obtained from (10) using $\frac{de_{\rm pv}}{dt}$ from (7) while considering $i_{L_1} = e_{i_{L_1}} + i_{L_1\rm ref}$ yields

$$\begin{aligned}\frac{di_{L_1\rm ref}}{dt} =\ & -k_{\rm PV}e_{i_{L1}} - \frac{C_1 k_{\rm PV}^2}{\gamma}e_{\rm PV} + \frac{1}{\gamma}\frac{di_{\rm PV}}{dt} \\ & - \frac{C_1}{\gamma}\frac{d^2 v_{\rm PVref}}{dt^2} - i_{L_1\rm ref}\frac{d\gamma}{dt}/\gamma.\end{aligned} \tag{12}$$

Consequently, the $e_{i_{L1}}$ time derivative in (11) is written as (13), taking into account (2) and (12)

$$\begin{aligned}\frac{de_{i_{L1}}}{dt} =\ & -\frac{v_p}{L_1} + \frac{v_{\rm PV}+v_p}{L_1}\gamma - \left(-k_{\rm PV}e_{i_{L1}} - \frac{C_1 k_{\rm PV}^2}{\gamma}e_{\rm PV}\right) \\ & - \left(\frac{1}{\gamma}\frac{di_{\rm PV}}{dt} - \frac{C_1}{\gamma}\frac{d^2 v_{\rm PVref}}{dt^2} - i_{L_1\rm ref}\frac{d\gamma}{dt}/\gamma\right).\end{aligned} \tag{13}$$

Taking into account the input voltage Lyapunov function (8), a recursively defined composite Lyapunov function (14), [28] with similar properties to (8), is considered for the inductor current

$$V_i = e_{\rm PV}^2/2 + e_{i_{L1}}^2/2. \tag{14}$$

Considering (7), (11), and (13), the Lyapunov function (14) time derivative is

$$\begin{aligned}\frac{dV_i}{dt} =\ & -k_{\rm PV}e_{\rm PV}^2 + e_{i_{L1}}\left[\frac{-v_p}{L_1} + \frac{v_{\rm PV}+v_p}{L_1}\gamma\right. \\ & + e_{\rm PV}\left(\frac{C_1 k_{\rm PV}^2}{\gamma} - \frac{\gamma}{C_1}\right) - k_{\rm PV}e_{i_{L1}} + \frac{C_1}{\gamma}\frac{d^2 v_{\rm PVref}}{dt^2} \\ & \left. -\frac{1}{\gamma}\frac{di_{\rm PV}}{dt} + i_{L_1\rm ref}\frac{d\gamma}{dt}/\gamma\right] = -k_{\rm PV}e_{\rm PV}^2 - k_{i_L}e_{i_{L1}}^2.\end{aligned} \tag{15}$$

To guarantee stability, the $\frac{dV_i}{dt}$ value must obey $\frac{dV_i}{dt} = -k_{\rm PV}e_{\rm PV}^2 - k_{i_L}e_{i_{L1}}^2$, thus the constant k_{i_L} must be positive so that the $\frac{dV_i}{dt}$ function is negative. Thus, equating the term relative to $e_{i_{L1}}$ (within the square brackets) to $-k_{i_L}e_{i_{L1}}^2$, the controller $\frac{d\gamma}{dt}$ in (16) is received

$$\begin{aligned}\frac{d\gamma}{dt} =\ & \frac{1}{i_{L_1\rm ref}}\left[\frac{v_p}{L_1}\gamma - \frac{v_{\rm PV}+v_p}{L_1}\gamma^2 - e_{\rm PV}(C_1 k_{\rm PV}^2 - \frac{\gamma^2}{C_1})\right. \\ & \left. + e_{i_{L1}}(k_{\rm PV} - k_{i_L})\gamma - C_1\frac{d^2 v_{\rm PVref}}{dt^2} + \frac{di_{\rm PV}}{dt}\right].\end{aligned} \tag{16}$$

The time integral of this equation returns the duty cycle that controls the dc–dc converter to obtain the maximum power regulating the dc–dc converter input voltage. As expected, the backstepping technique provided a virtual control $\frac{d\gamma}{dt}$ and the controller has to go back through an integrator.

B. DC–AC Power Converter Control

In the dc–ac inverter/rectifier, the control objective for the backstepping controller is to regulate the inverter input voltage, so that a telecom load can be supplied, as well as to source or sink ac sinusoidal current from the grid. The backstepping controller also needs two loops, an inner fast dynamics ac current loop

This article has been accepted for inclusion in a future issue of this journal. Content is final as presented, with the exception of pagination.

and an outer slow dynamics dc voltage loop. In order to keep the dc voltage nearly constant, from (4) the square of the input voltage must track a reference voltage squared to guarantee the energy balance within a grid voltage period, transferring the PV array excess power, if available, to the grid side, or sinking power from it in sunless or shadowing conditions. To source (or sink) ac current to the grid, the inductor current should track a sinusoidal reference current to ensure low harmonic injection into the electrical network ensuring low harmonic distortion.

To apply the backstepping method, the error of the outer loop voltage v_p must be defined as the difference between the square of voltage average value v_p^2 at the converter dc side and the square of its reference v_{pref}^2 value. This reference must be reached by the control to enforce v_{pref}^2 to v_p^2 to make any deviation vanish

$$e_{v_p^2} = v_{\mathrm{pref}}^2 - v_p^2. \tag{17}$$

The time derivative of the input voltage error $\frac{de_{v_p^2}}{dt}$ considering (4) is

$$\frac{de_{v_p^2}}{dt} = \frac{dv_{\mathrm{pref}}^2}{dt} - 2(i_p v_p - i_{L_2} v_R)/C_2. \tag{18}$$

As in the dc–dc converter, a similar Lyapunov function for the inverter input voltage is chosen and its time derivative is

$$\frac{dV_{vp}}{dt} = e_{v_p^2}\frac{de_{v_p^2}}{dt} = -k_{vp}\, e_{v_p^2}^2. \tag{19}$$

$\frac{dV_{vp}}{dt}$ is negative if k_{vp} is constant and positive. Taking into account this derivative and (18), a stabilizing function I_{L_2} can be obtained

$$I_{L_2} = \left(2i_p v_p - C_2 k_{vp} e_{v_p^2} - C_2 \frac{dv_{\mathrm{pref}}^2}{dt}\right) / (2v_R). \tag{20}$$

To separate the converter dynamics, this stabilizing function must relate the systems energy balance to the amplitude value I_{L2} of the i_{L2} current. Since $I_{L2\mathrm{RMS}}$ is the control parameter for the inner ac current loop, the fast dynamics trajectory can be foreseen considering that $i_{L_2\mathrm{ref}}$ must be a sinusoidal current in phase with v_R for $I_{L_2} > 0$, or with opposite phase for $I_{L_2} < 0$. This sinusoidal current reference can be written as $i_{L_2\mathrm{ref}} = I_{L_2} v_{Rpu}$ being a grid-synchronized unity amplitude sinusoid. To track this reference, the loop error is defined as

$$e_{i_{L2}} = i_{L_2\mathrm{ref}} - i_{L_2}. \tag{21}$$

A control law must be obtained using the time derivative of the error in (21)

$$\frac{dei_{L2}}{dt} = \frac{di_{L_2\mathrm{ref}}}{dt} - (\beta v_p - v_R)/L_2. \tag{22}$$

The Lyapunov function for the dc–ac converter inductor current is defined as

$$\frac{dV_{i_{L2}}}{dt} = e_{i_L 2}\frac{de_{i_L 2}}{dt} = -k_{i_{L2}} e_{i_L 2}^2. \tag{23}$$

$\frac{dV_{i_{L2}}}{dt}$ will be negative if $k_{i_{L2}}$ is constant and positive. Taking into account this derivative and (22), the modulation waveform

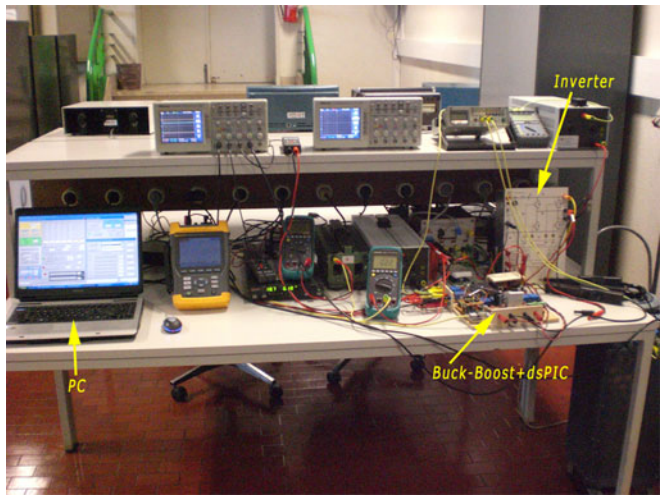

Fig. 4. Lab setup of the self-consumption PV system.

TABLE I
ELECTRICAL PARAMETERS OF SOLAR MODULE SIMULATOR AT 1000 W/M^2

Parameter	Values
Maximum power (P_{max}), in W	54 (+10%/−5%)
Maximum power voltage (V_{MPP}), in V	18.2
Maximum power current (I_{MPP}), in A	3
Open-circuit voltage (V_{OC}), in V	21.7
Short-circuit current ($I_{\mathrm{SC=I_1}}$), in A	3.31
Equivalent series resistance R_s, in Ω	0.2
Equivalent shunt resistance R_{sh}, in Ω	200

β is obtained

$$\beta = \left(L_2 \frac{di_{L2\mathrm{ref}}}{dt} + v_R + k_{i_{L2}} L_2 e_{i_L 2}\right) / v_p \tag{24}$$

where $v_p \neq 0$.

IV. EXPERIMENTAL SETUP AND RESULTS

Experimental tests have been developed in order to validate the proposed backstepping control under different conditions. An experimental platform [see Fig. 4] containing a subset of the distributed PV system has been built including one KC50TPV panel simulator [29] for a precise selection of the PV injected power. At nominal irradiance, the KC50T simulator outputs nearly 54 W. The panel simulator electrical parameters are listed in Table I.

The panel simulator feeds a buck–boost converter built using the MOSFET CSD19536KCS driven by FOD3180 driver, the diode MBR10200, $C_1 = 1000$ μF, $C_2 = 5700$ μF, and $L_1 = 20$ mH. The single-phase full-bridge inverter (4 CT60M-18F driven by IR2130, $L_2 = 13.1$ mH) is used to check the performance of the backstepping control. A transformer has been included between the dc–ac converter output and the weak LV 230-V 50-Hz grid due to the use of the telecom load. The telecom equipment has usually a nominal voltage of 48 V, although it can range from 36 to 75 V, and it needs a transformer to adapt the inverter ac output voltage to the grid voltage. LEM sensors

This article has been accepted for inclusion in a future issue of this journal. Content is final as presented, with the exception of pagination.

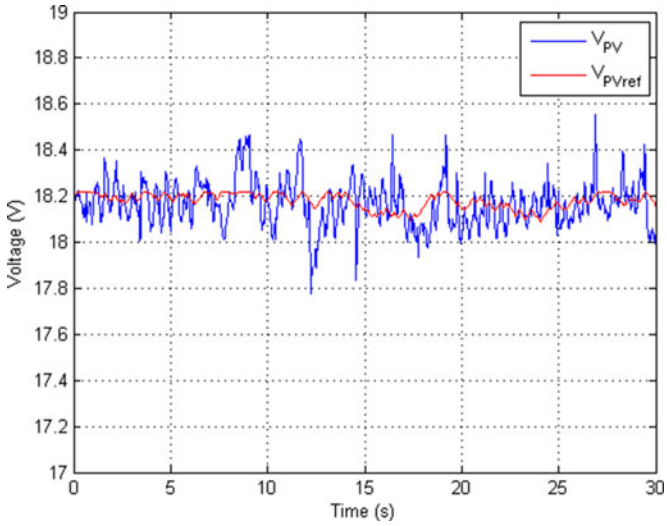

Fig. 5. MPPT operation.

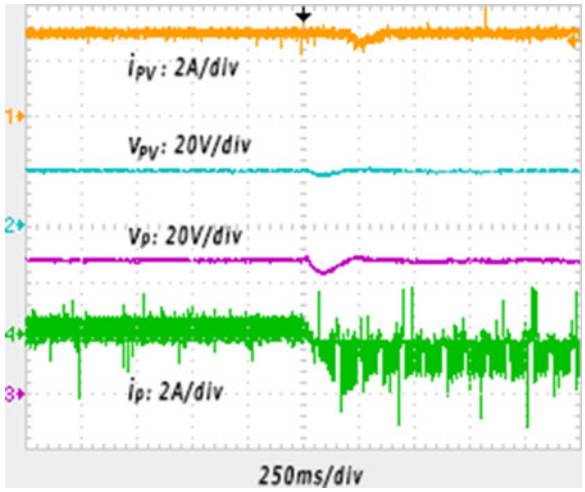

Fig. 6. Voltage and current waveforms when there is a change from inverter to rectifier.

were used in order to measure the required voltages and currents. The backstepping controller for the dc–dc converter and the inverter has been implemented in a low-cost dsPIC30F4011 microcontroller. The dsPIC was programmed to implement the constant frequency buck–boost modulator, the three level dc–ac converter modulator, the sampling of the voltages $v_{\rm PV}$, v_p, v_R, and currents i_{L1}, i_{L2}, 10 kHz, the grid synchronization, and the calculations needed in (16), (20), and (24). The values of the controller gains are: $k_{\rm PV} = 5$, $k_{i_L} = 75$, $k_{vp} = 4.7$, and $k_{i_{L2}} = 4600$.

The dsPIC is supervised, via a local Internet connection using a EM203 serial-to-Ethernet module, by a pc computer where a virtual instrument has been programmed using Visual Basic, to monitor the PV system operation and to generate the MPP reference voltage $v_{\rm PVref}$, using a method modified from [29] ensuring MPP voltage under changeable environmental conditions.

At the irradiance level of 1000 W/m^2, the measured input current and voltage at the input of the dc–dc converter were, respectively, 2.95 A and 18.2 V. Therefore, the power extracted from the PV simulator is 53.7 W. The maximum power the PV simulator outputs is 54.6 W [29]; therefore, the MPP is reached within a power efficiency of 98.3%. The buck–boost output voltage is 48.5 V and the output current is 1.02 A. The book–boost efficiency is 92% and the inverter output power at zero-telecom load is 43.2 W (88% inverter efficiency). The converter efficiencies are in the low side, especially the inverter, since it was not optimized for the telecommunication voltage operation range, but the backstepping MPPT efficiency is very good. The injected ac current total harmonic distortion (THD) is 1.6%. Fig. 5 shows the real MPPT operation, where the buck–boost input voltage $v_{\rm PV}$ tracks the changing reference voltage $v_{\rm PVref}$ at nearly 18.2 V.

A second steady-state condition has been tested at the irradiance level of 600 W/m^2. The buck–boost input current is 1.76 A and its input voltage is 18 V. The calculated MPP power is 31.7 W, being the efficiency of the backstepping MPPT near 99.9%. With no dc load, the inverter output power is 26.52 W and the efficiency of the whole system is about 84%. The ac grid current THD in this case is 1.7%.

In order to check the system dynamic performance, two different telecom type loads have been connected in parallel through switches to modify the power required by the load. Closing and opening of switches, the dc–ac converter can be changed from inverter operation to rectifier operation. If the power required by the load is chosen to be 25 W and the PV setup system outputs nearly 43 W, then the dc–ac converter must operate as an inverter, whereas if the telecom load needs 64 W, then the dc–ac converter must change to rectifier operation.

The experimental results of Fig. 6 show this change from inverter to rectifier. Fig. 6 presents the buck–boost input current $i_{\rm PV}$, the buck–boost input voltage $v_{\rm PV}$, the buck–boost output voltage v_p, and the dc–ac input dc current i_p, respectively. It is shown that the values of the converter input voltage and current and output voltage remain constant and the dc–ac converter dc current i_p changes from positive to negative when the inverter becomes a rectifier.

Fig. 7(a) shows the inverter ac output voltage v_R (at the line transformer secondary side) and the ac current i_{L2}. Fig. 7(b) is a zoom of (a) at the time change from inverter to rectifier. As can be seen, the ac voltage and current are in opposite phase in inverter operation, while they are in phase in rectifier operation. The ac voltage maintains its amplitude, but the current changes its amplitude and phase.

Fig. 8 shows the transformer ac voltage and current secondary-side waveforms and their values measured with a power quality analyzer Fluke 435. The dc–ac converter is operating in the inverter mode as the buck–boost supplies 48 W, and the load requires 25 W. Therefore, the excess 23 W can be injected in the grid at 30.9 V and 0.55 A, the inverter efficiency being 74%.

If the telecom load requires 64 W, then the dc–ac converter must operate as a rectifier. In this case, the grid injects 21 W

This article has been accepted for inclusion in a future issue of this journal. Content is final as presented, with the exception of pagination.

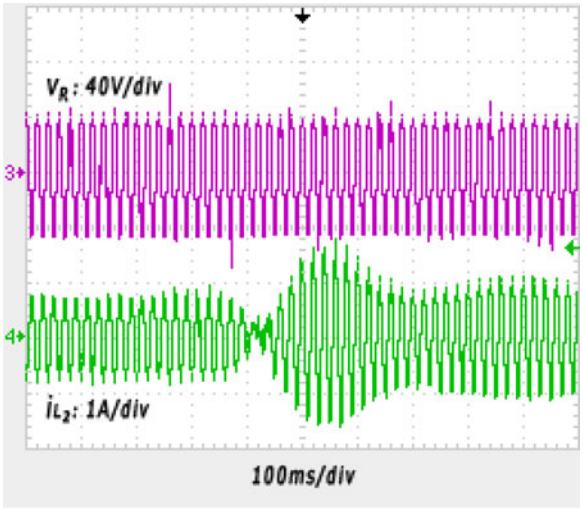

(a)

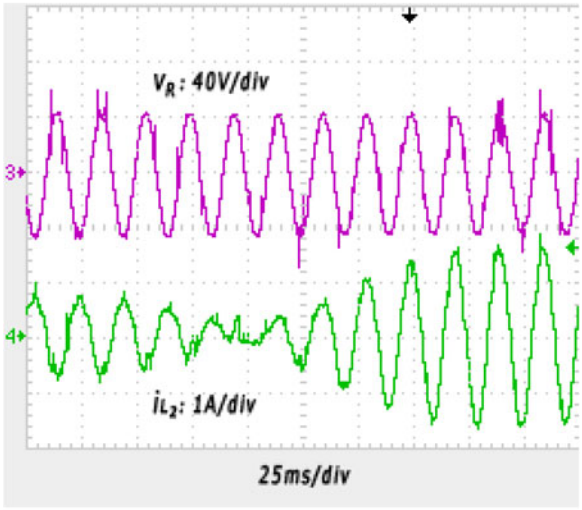

(b)

Fig. 7. (a) Voltage and current waveforms when there is a change from inverter to rectifier. (b) Center part zoom of (a).

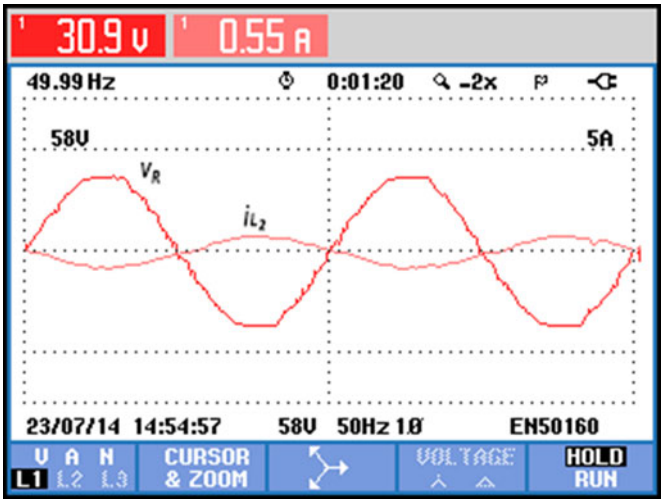

Fig. 8. Voltage and current waveforms when the load requires 25 W.

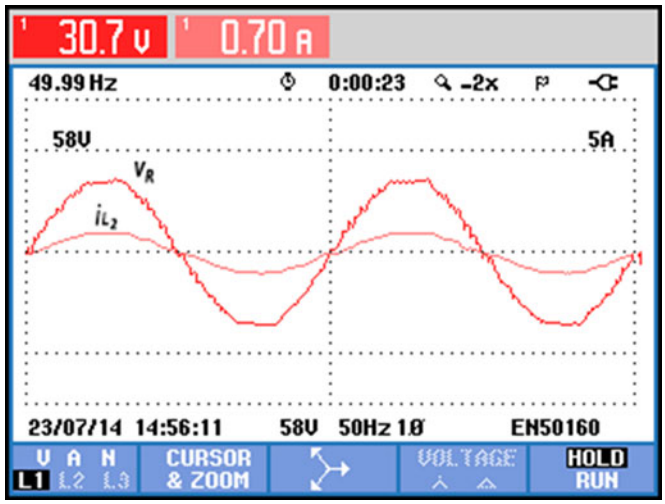

Fig. 9. Voltage and current waveforms when the load requires 62 W.

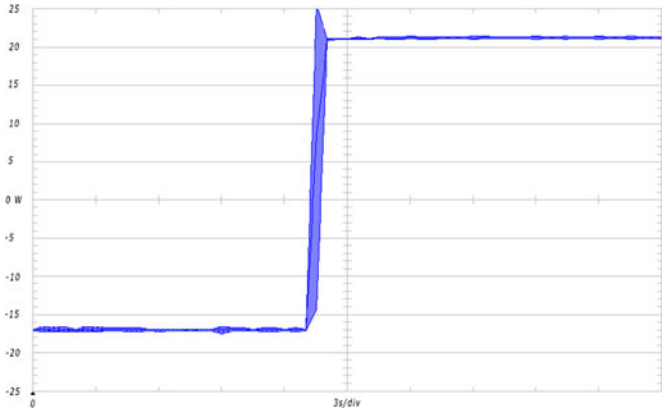

Fig. 10. DC–AC converter input power.

and the buck–boost supplies the maximum power nearly 43 W. Fig. 9 shows the ac voltage and current waveforms in phase, where the voltage is 30.7 V and the current is 0.7 A.

Fig. 10 shows the evolution of real-time power when the telecom load changes from 26 to 64 W and the PV supplies the maximum power 43 W. When the load requires 26 W, the dc–ac converter is working as an inverter and the PV excess power, in this case 17 W, is injected in the smart grid (-17 W in Fig. 10 inverter input power). Otherwise, the dc–ac converter works as a rectifier when the telecom load requires 64 W and the grid supplies 21 W [see Fig. 10] to the telecom equipment.

The current THD in all the cases is around $1.6\% \pm 0.1\%$. Practical robustness of the control concerning parameter changes has been also verified. The backstepping controller maintains its performance with capacitor C_2 ranging from 650 to 51000 μF, whereas the L_2 inductor can have values in the range from 4 to 40 mH.

V. Conclusion

This paper proposes a novel backstepping controller for a PV panel feeding a buck–boost converter, and dc linked to

This article has been accepted for inclusion in a future issue of this journal. Content is final as presented, with the exception of pagination.

a telecom load and a single-phase ac–dc converter connected to a smart grid, configuring a subset of a distributed hybrid photovoltaic power supply for telecom equipments within the self-consumption concept. This setup absorbs/injects nearly sinusoidal (THD = 1.6%, lower than the 3% required by the standards) grid currents at near unity power factor and the self-consumption can contribute to the smart grid peak power shaving strategy.

New nonlinear backstepping control laws were obtained for the input voltage of the buck–boost converter, thus achieving MPP operation (MPPT efficiency between 98.2% and 99.9%) and for the dc–ac converter regulating the dc telecom load voltage and controlling the ac grid current. All the control laws, fixed frequency converter modulators, voltage and current sampling, and grid synchronization have been implemented using a low-cost dsPIC30F4011 microcontroller.

Obtained experimental results show the performance of the PV self-consumption system using the backstepping control method. Results show the system dynamic behavior when the dc–ac converter changes operation from inverter to rectifier to adapt itself to the telecom load requirements. The robustness of the control laws has been tested as well. Capacitance of real capacitors can vary almost ten times around the rated value, while inductances can vary from 30% to nearly 300% of the rated value.

REFERENCES

[1] N. Femia, G. Petrone, G. Spagnuolo, and M. Vitelli, *Power Electronics and Control Techniques for Maximum Energy Harvesting in Photovoltaic Systems*. Boca Raton, FL, USA: CRC Press, 2013.

[2] A. Maki and S. Valkealahti, "Effect of photovoltaic generator components on the number of MPPs under partial shading conditions," *IEEE Trans. Energy Convers.*, vol. 28, no. 4, pp. 1008–1017, Dec. 2013.

[3] Epia Org. (2013, Jul.). Self-consumption of PV electricity—Position paper. [Online]. Available: http://www.epia.org/fileadmin/user_upload/Position_Papers/Self_and_direct_consumption_-_position_paper_-_final_version.pdf

[4] SunEdison. (2011, Nov.). Enabling the European consumer to generate power for self-consumption. [Online]. Available: http://www.sunedison.com/wps/wcm/connect/35bfb52a-ec27-4751-8670-fe6e807e8063/SunEdison_PV_Self-consumption_Study_high_resolution_%2813_Mb%29.pdf?MOD=AJPERES

[5] A. Nourai, R. Sastry, and T. Walker, "A vision & strategy for deployment of energy storage in electric utilities," in *Proc. IEEE Power Energy Soc. Gen. Meeting*, 2010, pp. 1–4.

[6] X. Yu, C. Cecati, T. Dillon, and M. G. Simões, "The new frontier of smart grids: An industrial electronics perspective," *IEEE Ind. Electron. Mag.*, vol. 5, no. 3, pp. 49–63, Sep. 2011.

[7] X. Ren, Z. Tang, X. Ruan, J. Wei, and G. Hua, "Four switch buck-boost converter for telecom DC-DC power supply applications," in *Proc. IEEE 23rd Annu. Appl. Power Electron. Conf.*, Feb. 2008, pp.1527–1530.

[8] M. Rashid *et al.*, *Power Electronics Handbook*, 3rd ed. Amsterdam, The Netherlands: Elsevier, 2011.

[9] P. P. Dash and M. Kazerani, " Dynamic modeling and performance analysis of a grid-connected current-source inverter-based photovoltaic system," *IEEE Trans. Sustain. Energy*, vol. 2, no. 4, pp. 443–450, May 2011.

[10] G.-K. Hung, C.-C. Chang, and C.-L. Chen, "Automatic phase-shift method for islanding detection of grid-connected photovoltaic inverters," *IEEE Trans. Energy Convers.*, vol. 18, no. 1, pp. 169–173, Mar. 2003.

[11] X. Lu, J. M. Guerrero, K. Sun, J. C. Vasquez, R. Teodorescu, and L. Huang, "Hierarchical control of parallel AC-DC converter interfaces for hybrid microgrids," *IEEE Trans. Smart Grid*, vol. 5, no. 2, pp. 683–692, Mar. 2014.

[12] T. Esram and P. L. Chapman, "Comparison of photovoltaic array maximum power point tracking techniques," *IEEE Trans. Energy Convers.*, vol. 22, no. 2, pp. 439–449, Jun. 2007.

[13] K. S. Tey and S. Mekhilef, "Modified incremental conductance algorithm for photovoltaic system under partial shading conditions and load variation," *IEEE Trans. Ind. Electron.*, vol. 61, no. 10, pp. 5384–5392, May 2014.

[14] T. Esram, J. W. Kimball, P. T. Krein, P. L. Chapman, and P. Midya, "Dynamic maximum power point tracking of photovoltaic arrays using ripple correlation control," *IEEE Trans. Power Electron.*, vol. 21, no. 5, pp. 1282–1291, Sep. 2006.

[15] A. El. Khateb, N. Abd Rahim, J. Selvaraj, and M. N. Uddin, "Fuzzy-logic-controller-based SEPIC converter for maximum power point tracking," *IEEE Trans. Ind. Appl.*, vol. 50, no. 4, pp. 2349–2358, Jul. 2014.

[16] Syafaruddin, E. Karatepe, and T. Hiyama, "Artificial neural network-polar coordinated fuzzy controller based maximum power point tracking control under partially shaded conditions," *IET Renew. Power Gener.*, vol. 3, no. 2, pp. 239–253, Jun. 2009.

[17] K. Sundareswaran, S. Peddapati, and S. Palani, "MPPT of PV systems under partial shaded conditions through a colony of flashing fireflies," *IEEE Trans. Energy Convers.*, vol. 29, no. 2, pp. 463–472, Jun. 2014.

[18] K. Ezal, Z. Pan, and P. V. Kokotovic, "Locally optimal and robust backstepping design," *IEEE Trans. Automat. Control*, vol. 45, no. 2, pp. 260–271, Feb. 2000.

[19] R. A. Freeman and P. V. Kokotovic, "Tools and procedures for robust control of nonlinear systems," Presented atin *Proc. IEEE 33rd Conf. Decision Control*, Nov. 2003, vol. 4, pp. 3458–3463.

[20] A. Luo, Y. Chen, Z. Shuai, and C. Tu, "An improved reactive current detection and power control method for single-phase photovoltaic grid-connected DG system," *IEEE Trans. Energy Convers.*, vol. 28, no. 4, pp. 823–831, Dec. 2013.

[21] S. Minaei, E. Yuce, S. Tokat, and O. Cicekoglu, "Simple realizations of current-mode and voltage-mode PID, PI and PD controllers," in *Proc. IEEE Int. Symp. Ind. Electron.*, Jun. 2005, vol. 1, pp. 195–198.

[22] A. D. Martin and J. R. Vazquez, "Backstepping controller design to track maximum power in photovoltaic systems," *Automatika*, vol. 55, no. 1, pp. 22–31, Jan. 2014.

[23] A. D. Martin, J. R. Vazquez, and R. S. Herrera, "Adaptive backstepping control of a DC-DC converter in photovoltaic systems," in *Proc. IEEE EUROCON*, Jul. 2013, pp. 949–955.

[24] F. Locment, M. Sechilariu, and I. Houssamo, "DC Load and batteries control limitations for photovoltaic systems," *IEEE Trans. Power Electron.*," vol. 27, no. 9, pp. 4030–4038, Sep. 2012.

[25] L. Jifang, T. Tianhao, and H. Jingang, "A neural network control strategy for multi-energy common dc bus hybrid power supply," in *Proc. Int. Symp. Power Electron. Elect. Devices Autom. Motion*, 2010, pp. 1827–1831.

[26] R. W. Wies, R. A. Johnson, A. N. Agrawal, and T. J. Chubb, "Simulink model for economic analysis and environmental impacts of a PV with diesel-battery system for remote villages," *IEEE Trans. Power Syst.*, vol. 20, no. 2, pp. 692–700, May 2005.

[27] M. Zahran, A. Dmowski, B. Kras, and P. Biczel, "PV battery wind-turbine public-grid hybrid power supply for telecom.-Equipment, system management and control," in *Proc. Intersoc. Energy Convers. Eng. Conf.*, 2000, vol. 2, pp. 1252–1260.

[28] H. K. Khalil, *Nonlinear Systems*, 3rd ed. Upper Saddle River, NJ, USA: Prentice Hall, 2002.

[29] M. Cardador, "Maximum power point tracker of grid connected photovoltaic systems using matrix converters," M.S. thesis, Dept. Elect. Comput. Eng., Instituto Superior Técnico, Universidade de Lisboa, Lisboa, Portugal, Jun. 2011.

Aranzazu D. Martin (S'13) was born in Bollullos del Condado, Huelva, Spain. She received the Degree in industrial engineering in 2008, and the Masters' degree in control engineering, electronic systems, and industrial computer science in 2001 from the University of Huelva, Huelva, Spain.

Since 2008, she has been collaborating with the Electrical Engineering Department, University of Huelva. She is currently working as a Researcher under the Formación del Profesorado Universitario (FPU) Grant. Her current research interests include renewable energy, distributed generation, power quality, and control systems.

This article has been accepted for inclusion in a future issue of this journal. Content is final as presented, with the exception of pagination.

J. M. Cano was born in Bollullos del Condado, Huelva, Spain. He received the degree in automatic and industrial electronic engineering, and the Masters' degree in automatic, robotics, and telematics from the University of Sevilla, Sevilla, Spain, in 2007 and 2008 respectively.

Since 2008, he has been collaborating with the Automatic Department, University of Sevilla. His current research interests include control systems, photovoltaics, unmanned aerial vehicles, and programming.

J. Fernando A. Silva (M'92–SM'00) received the Ph.D. degree in electrical and computer engineering from Instituto Superior Técnico, Universidade Técnica de Lisboa, Lisboa, Portugal, in 1990.

He is currently the Leader of the Power Electronics and Power Quality Group, Instituto de Engenharia de Sistemas e Computadores - Investigação e Desenvolvimento (INESC-ID) of Instituto Superior Técnico, Universidade de Lisboa, Lisboa. His research interests include pulsed power, advanced control of power electronics systems, and power quality.

Jesús R. Vázquez (M'14) was born in Huelva, Spain. He received the degree in electrical engineering from the University of Seville, Seville, Spain, in 1995, and the Ph.D. degree from the University of Huelva, Huelva, Spain, in 2004.

For one year, he was with the Electrical Department, Nissan Motor Ibérica S.A., Barcelona, Spain. Since 1996, he has been with the Electrical Engineering Department, Escuela Técnica Superior de Ingeniería, University of Huelva, Huelva. He teaches electric circuits, power quality, and photovoltaic systems, and his research interests include power quality, active power filters, renewable energy, distributed generation, and artificial network application.